ROYAL SOCIETY OF CHEMISTRY

PAPER

Check for updates

The efficacy of oleic acid treatment in passivating MAPbI₃ films†

Ghada Abdelmageed, [ID] [a] Rashad F. Kahwagi,[a] Joelle Korkomaz,[a] Anthony El-Halaby,[a] Adam F. G. Leontowich, [ID] [b,c] Sean Hinds[a] and Ghada I. Koleilat [ID] *[a]

Reliability, scalability, and excellent film properties with large crystals and low grain boundaries are essential for successfully commercializing perovskites in optoelectronic applications. Our previous reports introduced meniscus-guided blade coating, or shearing, which is referred to as one-step blade coating in the present study, as a promising method for depositing scalable perovskite films with millimetre-sized crystals, fulfilling two of the essential criteria. As a subsequent study, we investigated the stability of the films in response to humidity by employing a readily accessible hydrophobic molecule, oleic acid (OA), through surface passivation. We compared the quality of the surface treatment on films produced *via* one-step and two-step deposition methods utilizing spin and blade coating techniques while subjecting them to continuous exposure to high humidity levels. Initially, we applied OA to the films using spin-coating, which is the standard method for surface passivation. Our results prove that the film properties resulting from the deposition technique determine the effectiveness of the passivation process. A quick surface treatment using OA *via* spin coating can be highly effective for perovskite films with smooth surfaces and smaller grain sizes, in contrast to textured films with larger crystal sizes. By tailoring the surface treatment method from spin coating to dip coating, we demonstrated that OA can prolong the stability of perovskites for months under continuous high-humidity exposure.

1. Introduction

Metal halide perovskites (MHPs) with their various compositions have received enormous attention for their highly promising performance in solar cells.[1] The rapid progress of their reported power conversion efficiency (PCE) from 3.8% in 2009 to 27.0% in 2025 has been unprecedented, as evident in the National Renewable Energy Laboratory (NREL) efficiency chart.[2] However, the stability of the metal halide perovskites is highly dependent on their compositions and has been a major obstacle to the potential commercialization of perovskite solar cells.[3–6] Humidity, in particular, is a primary concern as it rapidly induces degradation in MHPs due to the high ionic nature of the material.[7,8] Many studies have focused on deciphering humidity-induced degradation pathways as a first step to tackle and solve this issue.[9–11] Methylammonium lead iodide ($CH_3NH_3PbI_3$, or $MAPbI_3$), arguably the most unstable perovskite composition, has been proposed to decompose into the hydrate intermediate compound according to eqn (1) as humidity permeates through the thin film grain boundaries.[12–16]

$$4CH_3NH_3PbI_3 + 2H_2O \rightarrow (CH_3NH_3)_4PbI_6 \cdot 2H_2O + 3PbI_2 \quad (1)$$

In this equation, isolated octahedra hydrated compound (PbI_6^{4-}) forms and subsequently PbI_2 separates and crystalizes, while volatile gases (*e.g.*, HI and CH_3NH_2 (MA)) form are released. In a detailed study, Song *et al.* have elucidated that humidity-induced degradation occurs by the forming of a low-dimensional, intermediate hydrated perovskite layer due to the dissolution of the Pb–I framework superficial layer and subsequent interaction with the organic species.[17] The intermediate hydrated layer may act as a protective barrier at the beginning of the exposure process, shielding the bulk from water molecules and suppressing the generation of free electrons caused by water doping. This could explain why controlled humidity can be beneficial.[18] Nonetheless, prolonged exposure to high levels of humidity is sure to promote an irreversible

[a]Department of Process Engineering and Applied Science, Dalhousie University, 1360 Barrington Street, Halifax, Nova Scotia, B3H 4R2, Canada. E-mail: ghada.koleilat@dal.ca

[b]Canadian Light Source Inc., 44 Innovation Boulevard, Saskatoon, SK, S7N 2 V3, Canada

[c]Department of Chemistry, University of Saskatchewan, Saskatoon, SK, S7N 5C9, Canada

†Electronic supplementary information (ESI) available. See DOI: https://doi.org/10.1039/d5nr00325c

decomposition of perovskite into a solid-state degradation byproduct (PbI$_2$) and volatile gaseous byproducts.[14] Alternatively, the degradation pathway develops through direct deprotonation of the organic cation, leading the perovskite to decompose directly into the degradation byproduct, bypassing the formation of an intermediate phase, as described by Lu *et al.*[19] They concluded that the termination of the MAPbI$_3$

surface and grain boundaries dictates the mechanism of the degradation pathway, whether through hydration or deprotonation, as illustrated in Fig. 1. Such termination can result from temperature preparation conditions where high temperatures may promote the breakage of the weak bonding of MA$^+$, leading to an increased presence of Pb-rich sites at the film's surface. MAI-terminated MAPbI$_3$ films, as those produced with
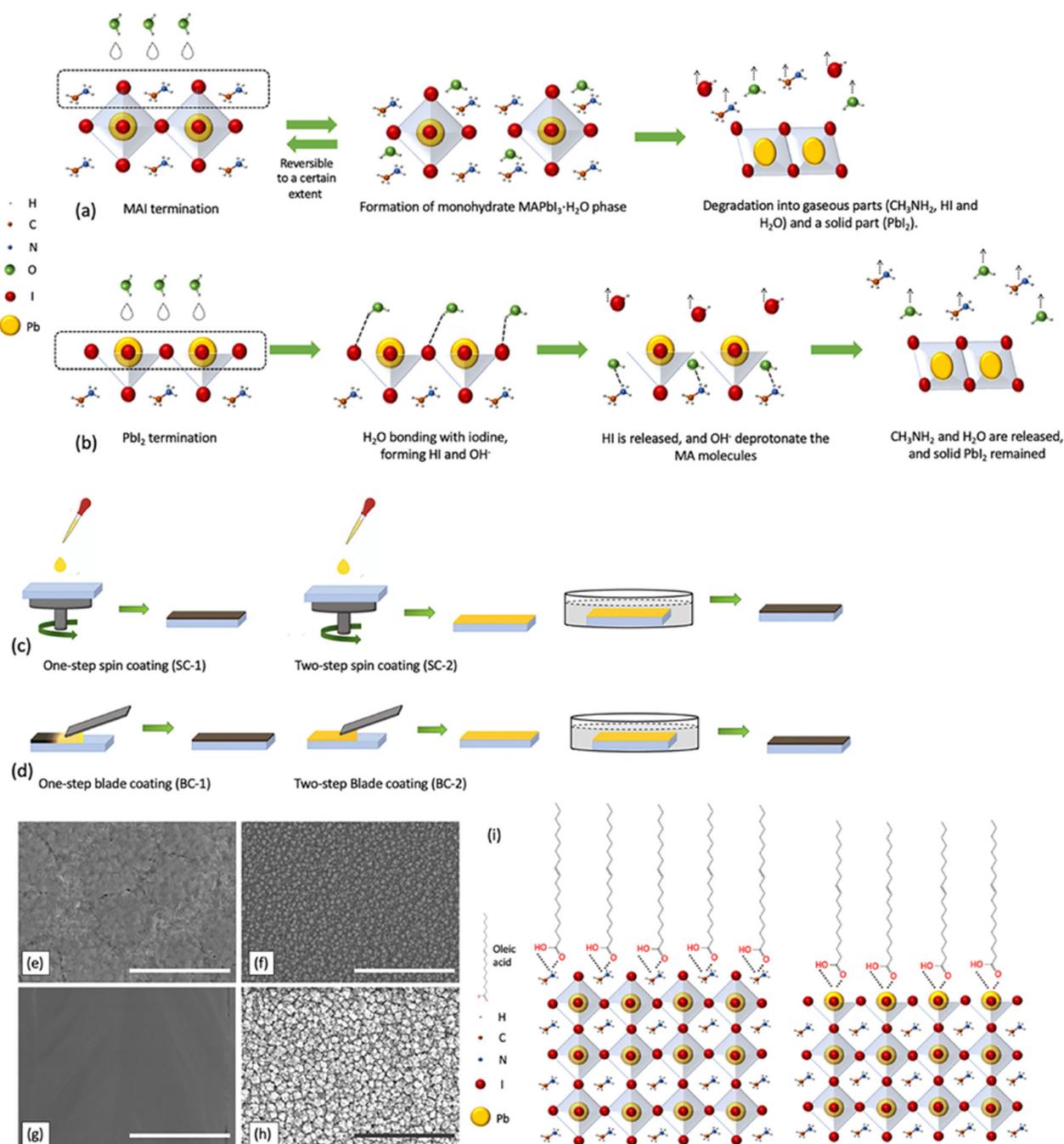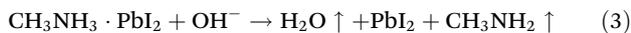

Fig. 1 Schematic illustrations of humidity-induced degradation pathways of MAPbI$_3$ surface layer with (a) MAI termination, (b) PbI$_2$ termination. Schematic illustrations of MAPbI$_3$ films preparation methods: (c) SC-1, and SC-2, (d) BC-1, and BC-2. SEM images (5k magnification, bar denotes 10 μm) of MAPbI$_3$ films prepared *via* different deposition methods: (e) SC-1, (f) SC-2, (g) BC-1, (h) BC-2. (i) Schematic illustrations of oleic acid molecules anchoring with the surface of MAPbI$_3$ films with different terminations.

low-temperature preparation conditions, were shown to degrade by allowing water molecules to penetrate and form hydrated compounds, similar to the interaction outlined in eqn (1). The reaction of the hydrated compound can be reversed with limited exposure to humidity. However, with prolonged exposure, the structure breaks down permanently into HI, CH_3NH_2, and PbI_2. The PbI_2-terminated $MAPbI_3$ films degrade directly into PbI_2 through an irreversible interaction of water molecules with iodine, producing volatile HI and OH^- ions that subsequently deprotonate MA^+ ions, as demonstrated in Fig. S1† and detailed in eqn (2) and (3).

$$CH_3NH_3PbI_3 + H_2O \rightarrow CH_3NH_3 \cdot PbI_2 + OH^- + HI \uparrow \quad (2)$$

$$CH_3NH_3 \cdot PbI_2 + OH^- \rightarrow H_2O \uparrow + PbI_2 + CH_3NH_2 \uparrow \quad (3)$$

Numerous potential solutions have been explored, including encapsulation and the implementation of chemical treatments, such as employing additives in solution and film surface passivation strategies.[20–24] Hydrophobic molecules, such as polyethylene terephthalate (PET), oleic acid, and polystyrene (PS), have been utilized to reinforce the long-term stability of perovskite.[22,25] Oleic acid ($C_{18}H_{34}O_2$) has been reported as an effective facile surface passivation ligand for perovskite and other nanocrystals as it prevents aggregation, improves chemical stability, and enhances optoelectrical properties.[26,27] Additionally, as a surface passivation treatment, oleic acid was reported to enhance perovskite solar cell efficiency by substantially reducing recombination.[25,28] Owing to its high hydrophobicity, the long-chained fatty acid theoretically should form a barrier to repel water molecules from the perovskite films surface thus suppressing that mechanism of degradation. A previous study reported improved stability for two-step spin-coated perovskite films and devices over 4 weeks of exposure to humidity.[25] While spin coating remains highly adopted in lab settings, blade coating, enables large-scale production with customizable surface coverage and is compatible with roll-to-roll (R2R) manufacturing essential for a wide range of applications, a feature that spin coating lacks. Furthermore, the deposition technique and its controls play a crucial role in the crystal growth process and the resulting thin film-forming properties. These properties, including morphology, crystal size, grain boundaries, and surface termination, significantly impact stability and morphological characteristics of the resulting films as demonstrated in our previous work.[29,30] Recently, we produced highly oriented millimetre-sized crystals by meniscus-guided blade coating.[29] We demonstrated that the pristine blade coated $MAPbI_3$ films with their macroscale crystal grains are inherently more stable that spin coated films when stored in nitrogen or ambient air over a one week period. Beyond that, we have not closely analyzed the properties of our films: to our knowledge no surface passivation has been reported to prolong the stability of the films.

Herein, we theorize that such vast changes in the film morphology and crystal formation process inherently alter the efficacy of widely reported, exclusively on spin-coated films, surface passivation treatments such as the facile oleic acid

surface treatment when films are exposed to severe continuous high humidity conditions and thus, require an in-depth evaluation and mapping of the films decomposition pathways. We initially hypothesized that films with large highly oriented crystals should in principle be vastly more stable than films with smaller polycrystalline regions: the results show that crystal packing, grain boundary depths and surface terminations directly impact the lifetime of the films exposed to severe humidity.

We used spin coating, the one-step method as well as the two-step method, both widely reported in the literature,[31] as comparative baseline methods of $MAPbI_3$ deposition techniques to be evaluated in conjunction with one-step and two-step blade coated $MAPbI_3$ films. Here the two-step refers to depositing PbI_2 first followed by MAI while the one-step refers to depositing both precursors simultaneously.[32] We assess the impact of the instantaneous oleic acid treatment on the various surfaces by analyzing degradation-induced changes in the perovskite films using various spectroscopic techniques, such as UV-Vis absorbance spectroscopy, photoluminescence (PL) spectroscopy, X-ray diffraction (XRD), and Fourier transform infrared (FT-IR) spectroscopy. We also rely on X-ray photoelectron spectroscopy (XPS) to elucidate the film's surface composition and deduce the degradation mechanics involved.

2. Experimental

2.1. Materials

All chemicals were used without further purification, including lead iodide (PbI_2, 99%, Sigma-Aldrich), methylammonium iodide (MAI, ≥99% anhydrous, Sigma-Aldrich), N,N-dimethylformamide (DMF, spectroscopic grade, Sigma-Aldrich), dimethyl sulfoxide (DMSO, anhydrous ≥99.9%, Sigma-Aldrich), diethyl ether (≥99.9%, Sigma Aldrich), 2-propanol (99.8%, Sigma-Aldrich), oleic acid (analytical grade, Supelco Inc., Millipore Sigma), and toluene (99.8%, Sigma-Aldrich). Borosilicate glass slides were used as substrates, and the dry aging conditions were achieved employing Drierite™ indicating absorbents (W.A. Hammond).

2.2. Preparation methods

Borosilicate glass slides were cut into 25 mm × 25 mm pieces, then cleaned by sonication in Triton solution, de-ionized water, acetone, and 2-propanol respectively for 20 minutes, and then dried using compressed N_2 gas. The dried slides were treated with ultraviolet ozone (UVO) for 20 minutes right before the perovskite deposition to enhance the wettability of the slides. The perovskite samples were prepared using spin and blade coating techniques (Fig. 1c and d) with the following details:

1 One-step spin coating (SC-1) deposition: the perovskite solution was prepared as follows: a 645 mg of PbI_2 and a 222 mg of MAI were dissolved in 1 mL DMF by stirring on a hotplate at 100 °C for 1 hour. Before deposition, the solution

was filtered using a syringe filter (PVDF, 22 μm pore size). 100 μL of the perovskite solution was spin coated in air on cleaned glass slides with speed of 3000 rpm for 25 seconds. 250 μL of chlorobenzene was dropped on the spinning slides in the final 10 seconds. Then, the films were transferred immediately to anneal on a hotplate (100 °C) for 10 minutes.

2 Two-steps spin coating (SC-2) deposition: PbI_2 (461 mg) was dissolved in DMF (1 mL) by stirring on a hotplate (80 °C, 400 rpm) for 30 minutes. The PbI_2 solution (50 μL) was spin-coated on the glass slide in air at 6000 rpm for 5 seconds, followed by an annealing step (100 °C) for 30 minutes in air. Then, the lead iodide films were dipped in the MAI solution for 5 minutes, as illustrated in Fig. 1b, converting them to $MAPbI_3$. The resultant perovskite films were rinsed with 2-propanol and dried on a hotplate (85 °C) for 2 minutes in air.

3 One-step blade coating (BC-1) deposition: 0.4 M of $MAPbI_3$ precursors solutions were prepared by dissolving PbI_2 (184 mg) and MAI (64 mg) in anhydrous DMSO (1 mL) in a N_2 filled glovebox. The solutions were stirred in the glovebox under dark conditions on a hotplate at 70 °C, 400 rpm, for 7 hours. Subsequently, the perovskite solutions were filtered (PVDF syringe filter, 0.22 μm). The deposition was performed in ambient atmosphere using a custom-made blade coating station that allow a heat assisted deposition. For the film formation, a 70 μL of the perovskite solution was blade coated on a clean glass slide at 160 °C, with a speed of 0.1 mm s^{-1}, and blade gap of 300 μm. The films were annealed for 20 minutes at 100 °C in inert atmosphere.

4 Two-step blade coating (BC-2) deposition: in this method, the PbI_2 and MAI solutions were prepared like in two-step spin coating. For the deposition, a 50 μL of PbI_2 solution was blade coated at 100 °C, with a speed of 1 mm s^{-1}, and blade gap of 300 μm and subsequently annealed for 30 minutes at 100 °C. Next, the as prepared PbI_2 films were dipped in the MAI solution for 5 minutes, and the resultant perovskite films were rinsed and dried in air in the same details as two step spin coating (SC-2).

2.3. Surface passivation treatment and aging procedure

Equal amounts of toluene and oleic acid were stirred for 10 minutes in air, then 50 μL of the prepared solution was spin-coated on $MAPbI_3$ films for 10 seconds at 0 rpm (loading time) then at 25 seconds at 6000 rpm in air, followed by drying on a hotplate for 5 minutes at 70 °C in air. For dip coating, the films were dipped in the oleic acid solution for 10 minutes. Then the films were rinsed briefly with toluene to remove excess oleic acid molecules, dried on the hotplate for 5 minutes at 70 °C, and stored overnight under vacuum to ensure the complete dryness. To test the effectiveness of the surface passivation treatment against high humidity levels, we followed a previously reported method in which the untreated and treated samples were placed inside an airtight container with saturated sodium chloride solutions in dark conditions to avoid any photoinduced degradation. In such a method, water evaporates from the salt solution inside the enclosure to reach equilibrium at relative humidity levels of around 76% at room temperature.[33,34] The salt mixtures were monitored throughout the experiment and replenished when needed to ensure the steadiness of the humidity levels. Duplicate control and treated samples were stored in dark, dry conditions using indicating Drierite™ to monitor any parasitic effect of oleic acid on the perovskite stability.

2.4. Characterization techniques

The humidity-induced structural changes of the perovskite films were examined using UV-Vis absorbance spectroscopy (Agilent Cary 60 Spectrophotometer), and photoluminescence (PL) spectra were measured using a Cary Eclipse fluorescence spectrometer. The excitation wavelength used was 532 nm, with a penetration length of 80 nm at the $MAPbI_3$ surface, and the films were measured from the film side.[35] X-ray diffraction (XRD, Bruker D8 Advance X-ray diffractometer, Cu Kα source, λ = 1.5406 Å), and Fourier Transform Infrared (FT-IR) spectroscopy (Agilent Cary 630 FTIR). Grazing-incidence wide-angle X-ray Scattering (GIWAXS) was conducted on perovskite films at the Brockhouse X-ray Diffraction and Scattering Sector Wiggler Low Energy (BXDS-WLE) beamline of the Canadian Light Source (CLS) synchrotron, using a photon energy of 15.1 keV (λ = 0.81931 Å).[36]

In addition, the morphology and surface properties of the samples were analyzed using scanning electron microscopy (SEM, Hitachi S-4700, cold field emission), and X-ray photoelectron spectroscopy (XPS, Thermofisher Multilab 2000). The XPS instrument had a magnesium anode (1253.6 eV) with the sample chamber under pressure range from 6×10^{-10} to 2×10^{-9} Torr. The samples' exposure to the X-rays was limited to less than 20 minutes. All measurements were conducted in dark conditions to prevent any additional photoinduced degradation mechanism. The X-ray penetration depth into the film was calculated to be <10 nm. All XPS data analysis was performed using CasaXPS software (ver. 2.3.23).[37] Background subtraction was performed using a Shirley background and peak fitting uses symmetric Gaussian/Lorentzian peak shapes. The elemental atomic concentrations of the perovskite surface were computed from ratios of XPS peaks intensities after appropriate normalization *via* atomic sensitivity factors.[38,39]

3. Results and discussion

We prepared the perovskite film samples through two different deposition techniques, namely blade coating and spin coating, either *via* one-step or two-step methods as illustrated in Fig. 1c and d. Each preparation method resulted in different film-forming properties with different grain sizes, revealed in scanning electron micrographs in Fig. 1e–h and S4.† The blade coating method produced sizably larger crystal sizes compared to spin coating, with one-step blade coating, in particular, producing the biggest grain size of all. The large crystals created by one-step blade coating agree with previous studies that proved that meniscus-guided blade deposition can yield millimeter-sized crystal grains.[29,30,40]

The samples (SP-1, SP-2, BC-1 and BC-2) were very briefly surface treated (<10 s) with oleic acid and then subjected to high humidity levels (∼76% RH). The passivation occurs by binding the carboxyl group (–COO⁻) of oleic acid to surface Pb^{2+} and/or $CH_3NH_3^+$ sites, depending on the surface termination of the perovskite film. We opted for such a brief chemical treatment to investigate the efficacy of the OA molecule's adherence to the film's surface only, thus mainly shielding the top layer.

Fig. 2 illustrates the changes in UV-Vis absorbance and PL spectra of the samples over time. Results show an enhancement in the stability of the treated samples, except BC-1, which fully degraded through exposure to humidity within one week and no longer retained the characteristic absorption onset around 770 nm, representative of the MAPbI₃ bandgap. BC-2 samples were fully degraded after four months; meanwhile, the spin-coated samples were fully degraded after six months of continuous exposure. All untreated control samples degraded after one week (Fig. S1†). We theorize that the difference in crystal size might have a critical role in the viability of surface passivation treatment, especially a brief treatment, allowing for trapped active spots that can interact with humidity and initiate degradation at a much faster pace. Not only that, when closely examining the SEM images of the BC-2 *versus* the spin-coated samples, the grains while similar in size are protruding through the surface and exhibit more fissures than the smooth spin-coated films, resulting in a faster degra-

dation within 4 months in place of 6 months as indicated by Fig. 2d.

We note that all samples after passivation registered higher PL intensity with a nominal repeatable blue-shifted peak. After OA treatment, the PL peaks shifted from 780, 771, 786, and 778 nm to 776, 768, 779.5 and 775 nm for SC-1, SC-2, BC-1, and BC-2 samples, respectively. A consistent observed blue shift indicates the passivation of radiative trap states at the surface level of the samples, as illustrated in Fig. 2e.[35,41] Such a phenomenon was described in previous works, as the spontaneous radiative recombination from defects resulting in a red shift in the emission peak, and the passivation of these defects leading to a blue-shifted emission peak denoting a radiative band edge transition.[35] Peaks from all untreated films vanished after 1 week of continuous exposure to humidity, consistent with the absorbance results, including that of the treated one-step blade coating film. The aged, treated films of SC-1, SC-2 and BC-2 showed PL spectra with peaks at 768, 768 and 773 nm, respectively. A slight blue shift in the aged peaks of SC-1 and SC-2 samples could be either due to degradation and the formation of PbI₂ or due to an additional passivation effect from water molecules that are not yet enough to induce degradation but rather in small quantity reported to be beneficial.[17,42] Upon further exposure, the films showed complete degradation after six months for the SC-1 and SC-2 films and after 4 months for the BC-2 films. This is in line with our earlier observations; while crystal and grain size matter, morphological roughness also plays a role.
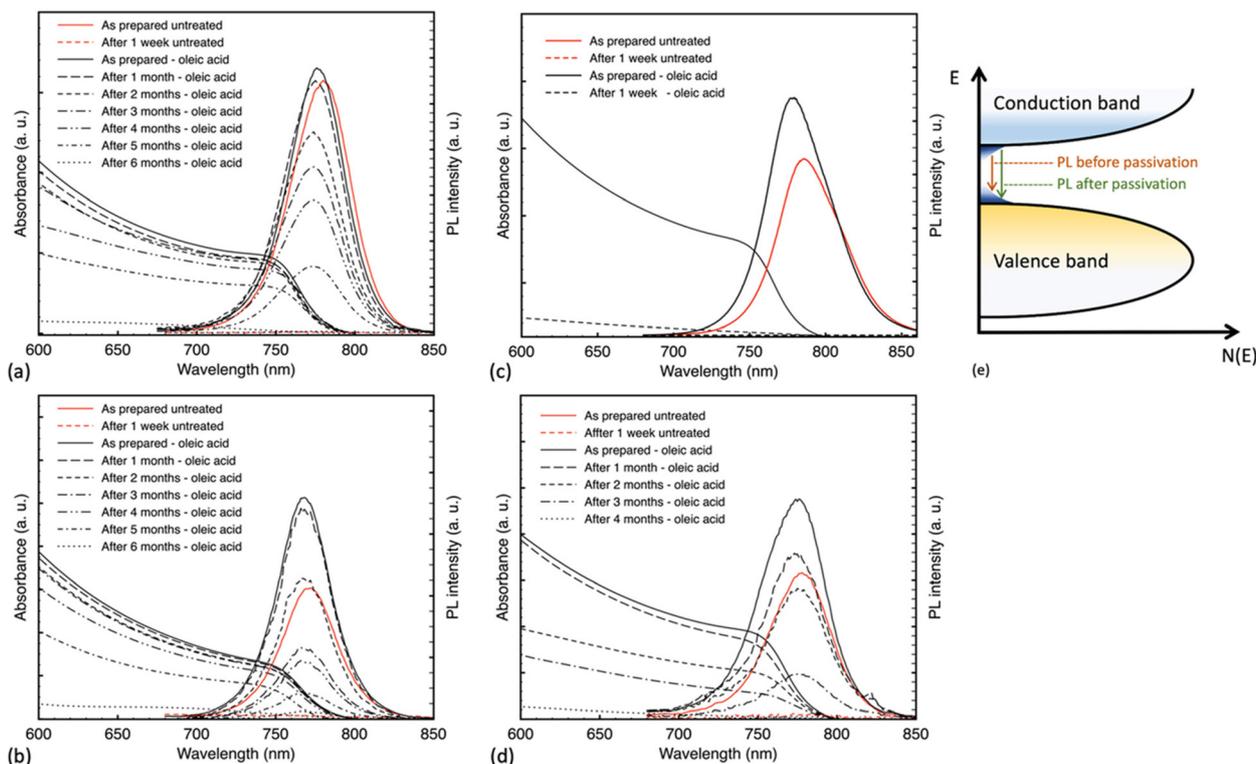

Fig. 2 UV-Vis absorbance and PL spectra of MAPbI₃ films treated with oleic acid and aged at ≈76% RH (a) SC-1, (b) SC-2, (c) BC-1, (d) BC-2. (e) A schematic illustration of the blue shift in PL after passivation.

X-ray diffraction analysis was performed to investigate the humidity-induced structural changes of the perovskite films; Fig. 3 depicts the difference in their crystal structure, with surface passivation of oleic acid, during the aging process in high humidity conditions. All freshly prepared samples showed the characteristic perovskite peaks at 2θ around 14.14°, 28.50°, and 43.34° assigned to the (110), (220), and (330) lattice planes, indicating a tetragonal crystal structure.[30] The results indicated the slight formation of hexagonal PbI_2 with a signature peak at 2θ around 12.65° by the end of the first month in SC-1 and BC-2 samples. The SC-2 sample did not show any rise of the PbI_2 peak for the first month of humidity exposure. Nevertheless, with continuous exposure, the PbI_2 characteristic diffraction peak gradually increased in these samples, while $MAPbI_3$ peaks decreased. Additionally, BC-1 was converted to a mixture of hydrated intermediate phase, as evidenced by the peaks at 8.22° and 10.79°, and $MAPbI_3$ after three days of aging, and by the end of the first week, it degraded completely to 100% intermediate phase.[12,43] The peak at 8.22° has been reported for forming 2D phases in perovskite, which is consistent with the formation of low-

dimension hydrated phases.[17,44] The diffraction patterns of the untreated samples are shown in Fig. S2:† they all completely degraded to PbI_2 except for the one-step blade coating, which degraded to a mixture of intermediate phase and PbI_2. This implies that deprotonation of the organic cation is the dominant degradation mechanism for the samples, except for BC-1, which decomposes *via* bulk hydration. Based on the results above, oleic acid improved the stability of the prepared films, except for those coated using the one-step blade method. To further investigate the structural changes in the films during aging, we analyzed the GIWAXS patterns of the aged films treated, as shown in Fig. 4. The samples exhibit lattice planes of (110) and (220) peaks at a momentum transfer $q \approx 1.0$ and 2.0 Å^{-1}.[45] The spin-coated films display homogeneous arcs, indicating isotropic distribution. In contrast, the blade-coated films exhibit a higher degree of preferential crystallographic orientation, characterized by partial arc segments and more pronounced Bragg spots.[30] After aging in humid conditions, the one-step blade-coated film completely degraded in one week, with the only patterns being strong arcs at $q \approx 0.5$ and 0.75 Å^{-1} assigned to the hydrated intermediate
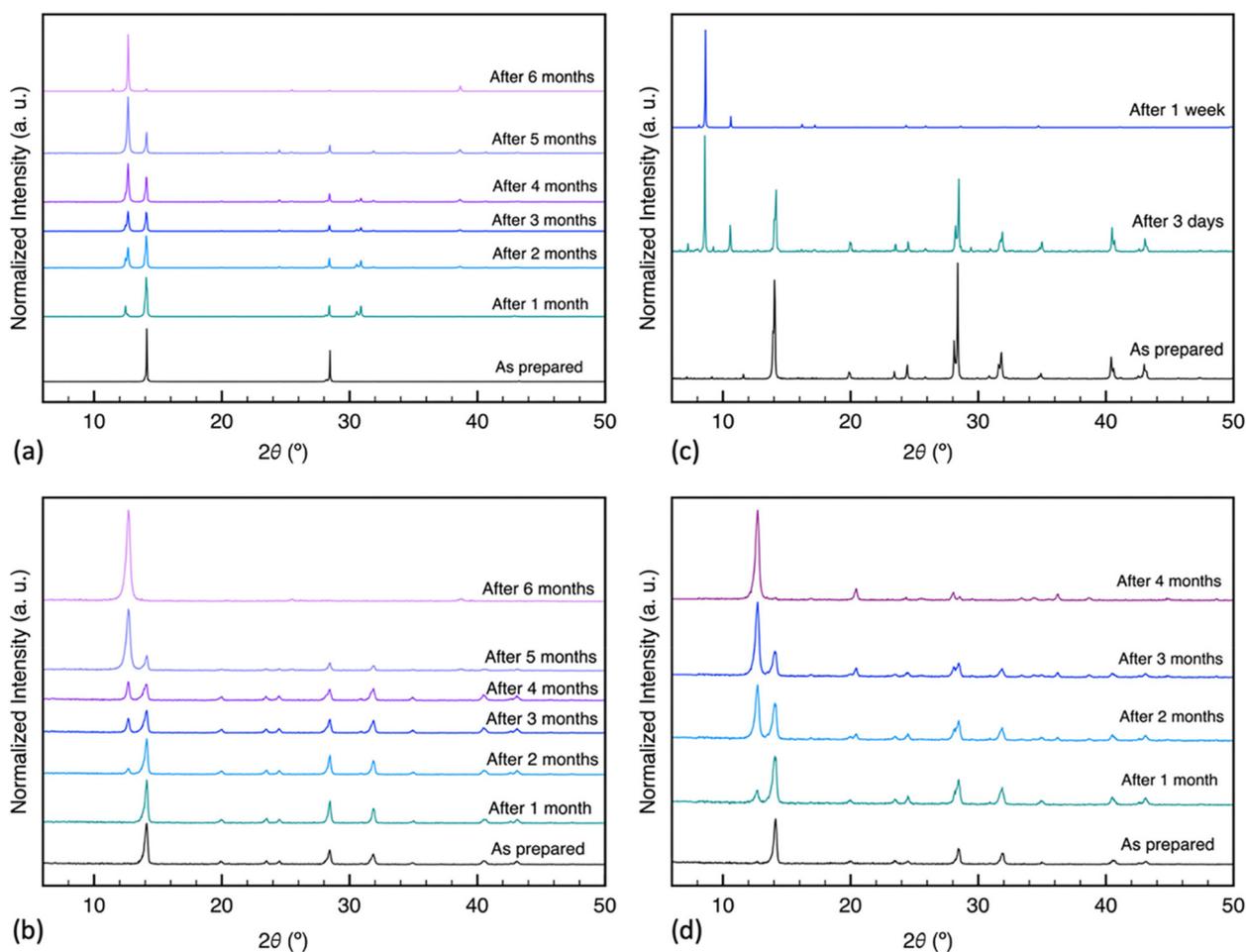

Fig. 3 X-ray diffraction patterns (λ = 1.5406 Å) of $MAPbI_3$ films prepared *via* different deposition methods, treated with oleic acid and aged at ≈76% RH: (a) SC-1, (b) SC-2, (c) BC-1, (d) BC-2.
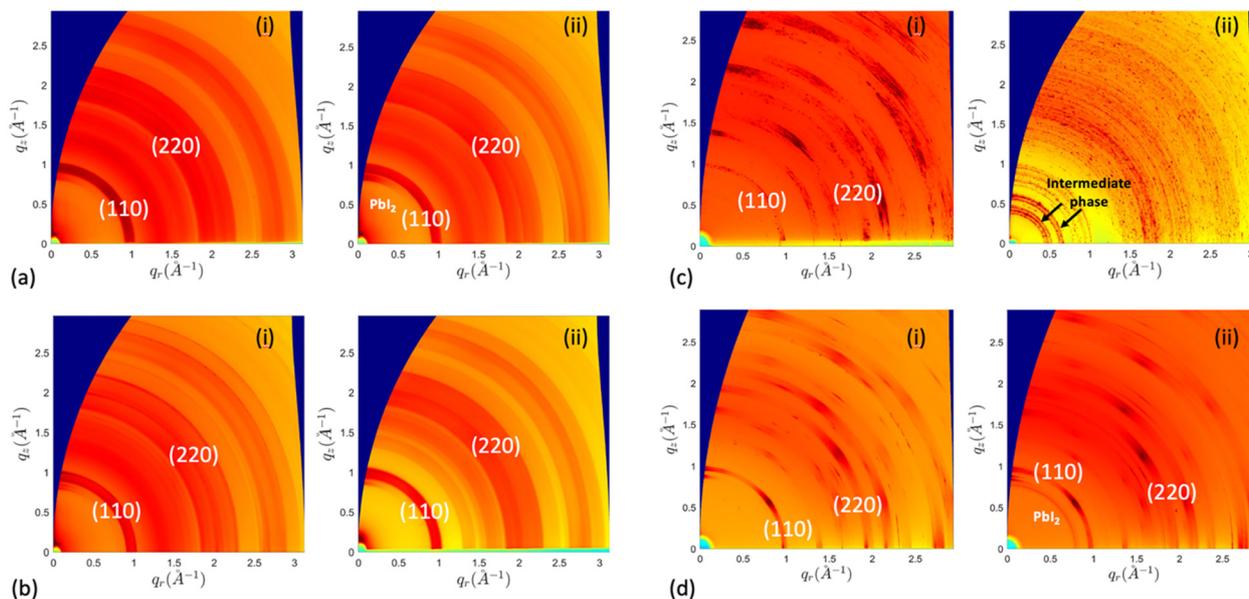
Fig. 4 GIWAXS patterns of MAPbI$_3$ films treated with oleic acid ((i) as prepared, and (ii) aged) prepared via different deposition methods and aged at ≈76% RH: (a) SC-1, (b) SC-2, (c) BC-1, (d) BC-2. The incidence angle θ was 0.15° for all measurements.

phase.[46–48] The two-step blade-coated, and the spin-coated samples were the most stable after 1 month of exposure. The one step spin coated sample showed a slight increase in PbI$_2$ (100) peak intensity at $q \approx 0.9$ Å^{-1} and the two-step blade-coated sample showed a more distinct peak. To test the reversibility of this intermediate phase of BC-1 sample, we heated the samples that degraded to 100% intermediate phase on a hotplate at 100 °C for 30 minutes in air. As seen in Fig. 5a, the degraded treated film did not show a significant change in the UV-vis absorbance spectrum after heating, just a minute recovery of the perovskite absorption onset as seen in the inset, implying very limited reversibility. The XRD results in Fig. 5b show that upon heating, the untreated film converts to mostly

PbI$_2$ with residues of perovskite, while the treated film converts to only residues of perovskite with no PbI$_2$ formation. This indicates that oleic acid fully inhibits the deprotonation process: most of the perovskite leached out of the film during the hydration phase, and only the remnants were recovered upon heating.

To probe the chemical composition of the hydrated phase, the molecular structure of the samples under degradation was investigated by examining their FTIR spectra. The pristine samples showed strong vibrational bands at 717 and 900 cm^{-1} for CH$_2$ stretching and CH$_3$ rocking respectively.[49,50] Other weaker bands were observed at 1468, 1564, 2110 and 3100 cm^{-1} assigned to C–H scissoring, N–H bending, C–N
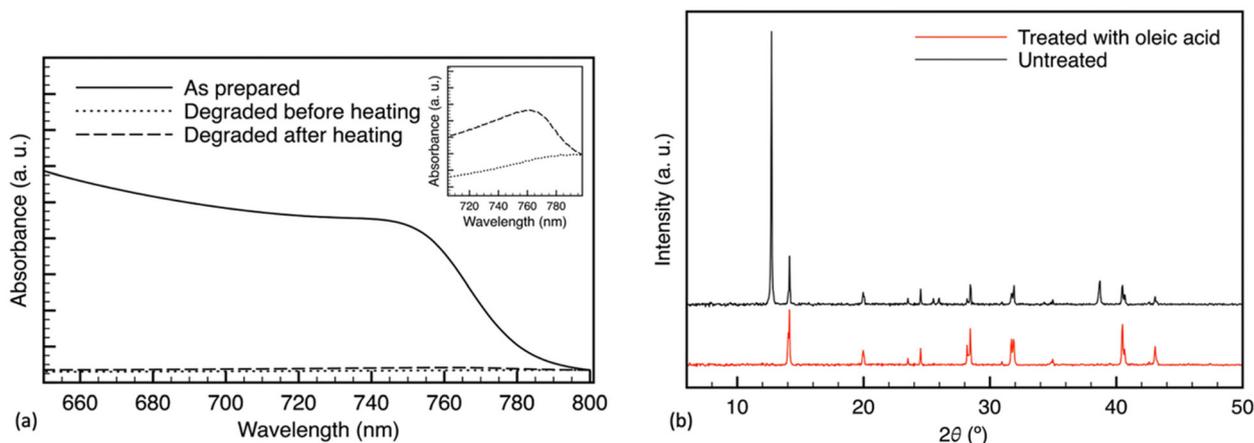

Fig. 5 (a) UV-Vis absorbance of a BC-1 sample treated with oleic acid before and after the degradation process and then the subsequent heating process. (b) X-ray diffraction patterns (λ = 1.5406 Å) of the heated BC-1 samples after the degradation process and then the subsequent heating process.

stretching and N–H stretching respectively.[51–54] Samples prepared *via* blade coating showed bands in the range between 1300 to 1700 cm^{-1} more prominently than the spin-coated films, which could be due to the difference in the preparation

processes and surface morphology. The samples treated with oleic acid showed vibrational bands at 1280, 1720, 2850 and 2920 cm^{-1} assigned to C–O stretching, C=O stretching, symmetrical CH_2 stretching and asymmetrical CH_2 stretching
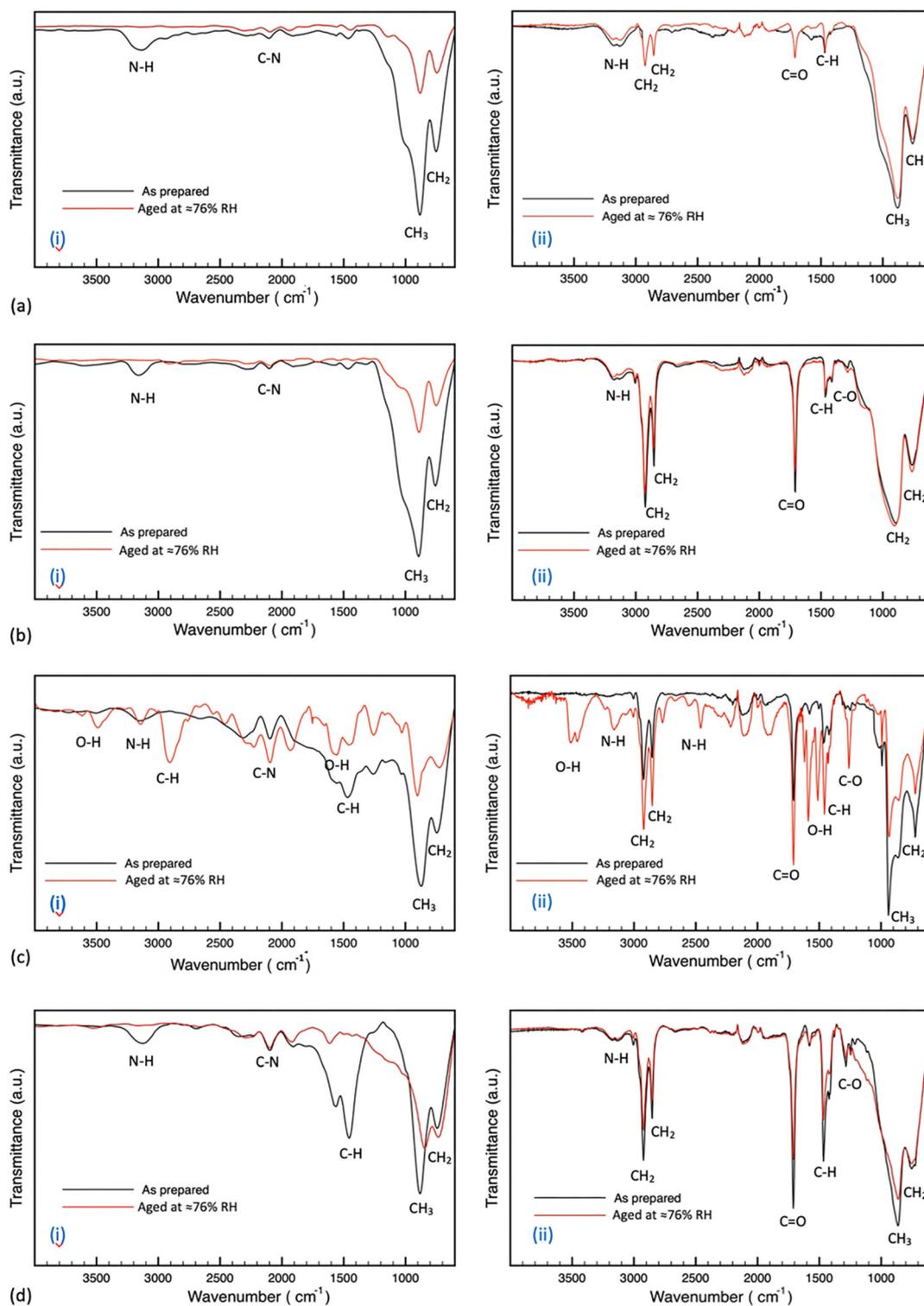

Fig. 6 FTIR spectra of MAPbI$_3$ films prepared *via* different deposition methods and aged at ≈76% RH: (a) SC-1, (b) SC-2, (c) BC-1, (d) BC-2. The graphs marked with (i) denote the untreated control samples, and (ii) denotes samples treated with oleic acid.

respectively.[55] The FTIR spectrum of oleic acid is provided in the ESI (Fig. S3).† The results in Fig. 6 indicate that all untreated samples showed significantly reduced intensity in vibrational bands characteristic of the organic cation, which is consistent with the degradation mechanism of the MA$^+$ from the perovskite structure.[56] All untreated samples, except the one-step blade coating film, showed no new vibrational bands with humidity exposure. The aged pristine one-step blade coating film showed both decreased intensity of the organic cation bands and the creation of new bands at 1425, 1925, 2464, 2550, 2906, 3485 and 3612 cm^{-1} due to the formation of hydrated intermediate compounds such as –COO, and O–H stretching modes.[57] The treated films, except one-step blade coating, did not show significant change with humidity exposure. The treated one-step blade coating (BC-1) film showed decreased band intensities of the vibrational modes of the CH$_2$ and CH$_3$ functional groups; however, it showed stronger intensities of O–H in plane stretching at 1452 cm^{-1}, the carbonyl functional group at 1705 cm^{-1}, –COO$^-$ stretching at 1582 cm^{-1} and N–H stretching at 2857 and 2928 cm^{-1}.[58] In addition, new bands formed including C–O stretching at 1258 cm^{-1}, antisymmetric stretching –COO$^-$ at 1617 cm^{-1}, N–H stretching modes at 2464, 2551, 2766 cm^{-1}, and O–H

stretching modes at 3157, 3455 cm^{-1}.[57–60] Such FTIR band changes of a hydrated perovskite are in agreement with a previous study performed by Gan *et al.*[57] These results demonstrate that the one-step blade coating samples degrade by forming hydrated intermediate compounds with and without the surface passivation treatment. In addition, BC-1 samples show a weak peak around 1020–1030 cm^{-1} assigned to S═O stretching band that is characteristic to DMSO, denoting the slight formation of MAI-PbI$_2$-DMSO intermediate phase with the preparation step, concurring with the XRD results.[61,62] These results are consistent with our previous conclusion that SC-1, SC-2, and BC-2 films indeed degrade directly to PbI$_2$ through the evaporation of the organic cation, while BC-1 degrades through the formation of hydrated and metastable intermediate compounds.

To further understand the inadequacy of the surface passivation treatment in one-step blade-coated perovskite films, we proceeded to analyze the surface properties of our films. Rather than merely considering crystal and grain size as key factors, we investigated whether bond terminations affected the treatment efficacy. We quantified the atomic concentration percentages of the elements at the perovskite surface level *via* XPS measurements presented in Fig. 7. The XPS survey spectra (see ESI, Fig
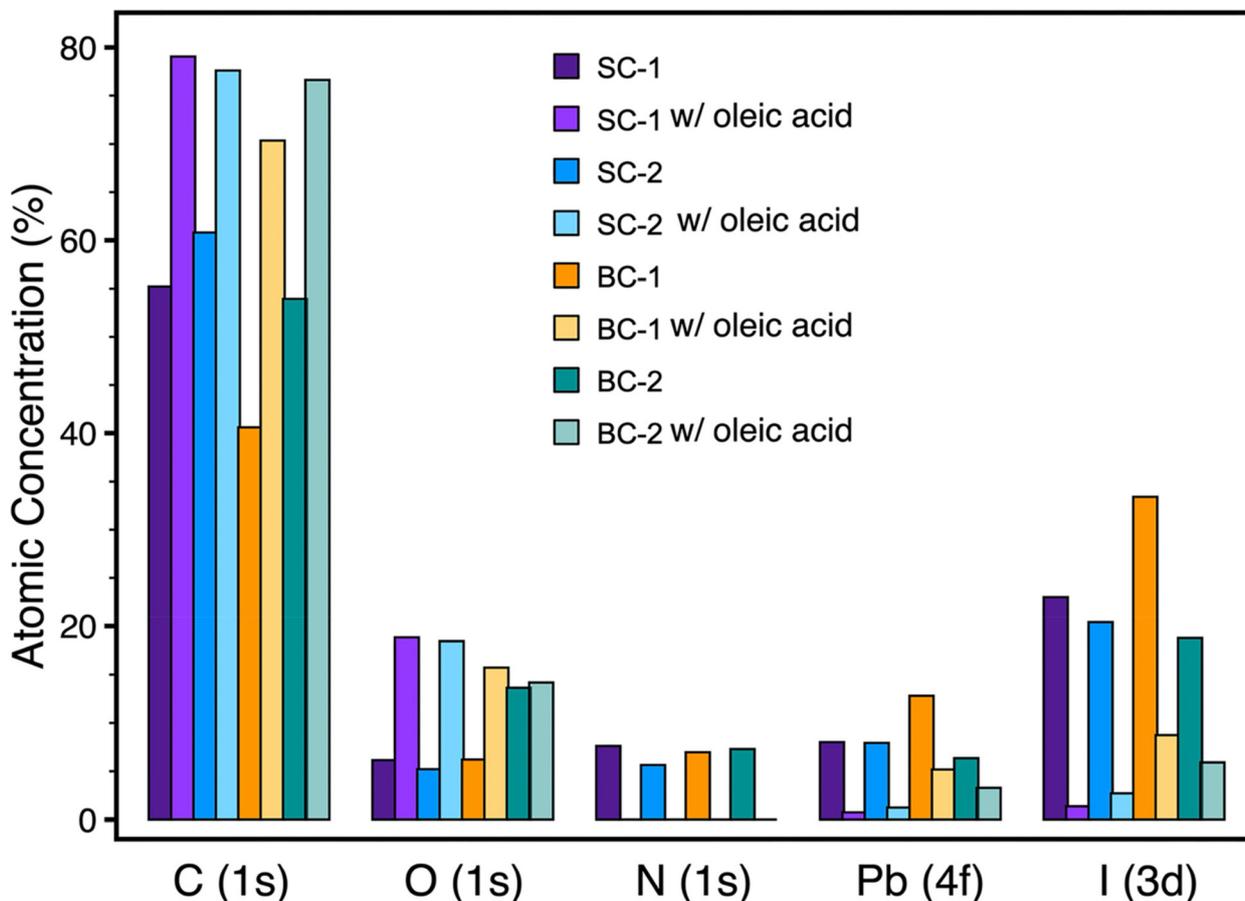

Fig. 7 Atomic concentration percentages of C, O, N, Pb, and I at the surface level of the MAPbI$_3$ films, derived from X-ray photoelectron spectra.
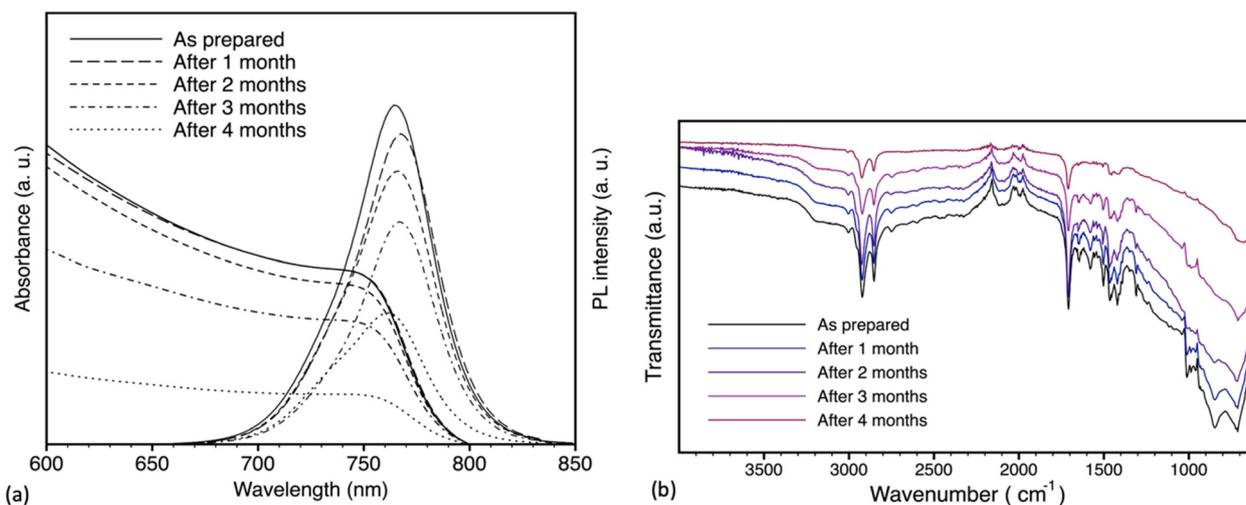
Fig. 8 (a) UV-Vis absorbance and PL spectra and (b) FTIR spectra of BC-1 film treated with oleic acid dipping method, and aged at ≈76% RH.

S6†) for the MAPbI$_3$ perovskite films reveal peaks for O, N, and C at binding energies of approximately 532, 401, and 284.6 eV, respectively. Both I and Pb exhibit doublet peaks due to spin–orbit splitting, appearing at around 618, 630, 137, and 143 eV, respectively.[63] The oxygen peak can be explained by the propensity of MAPbI$_3$ films to undergo surface oxidation and the formation of PbO/Pb(OH)$_2$ like states with terminated Pb dangling bonds, as reported by Rocks *et al.*[63] However, no secondary phase of PbO was detected in the XRD measurements, which aligns with prior studies reporting an O peak in XPS without evidence in XRD.[63,64] The results shown in Fig. 7 indicated a significant difference between the one-step blade-coated (BC-1) film and the other films, in their as-prepared condition, displaying notably a lower C concentration and higher Pb and I concentrations, indicating more PbI$_2$ termination. This concurs with the study suggesting that annealing at high temperatures promotes MAI desorption at the surface level.[19] This may explain the ineffectiveness of oleic acid in adequately passivating the iodine-rich surface. After passivation, we observed a sharp increase in the C and O atomic concentrations due to the presence of oleic acid (C$_{18}$H$_{34}$O$_2$). The formation of the surface passivation layer decreased the atomic concentrations of N, Pb, and I through the few nanometers tested through XPS. We thought to tailor the treatment to increase its efficiency on BC-1 films: we know that BC-1 films are prone to form thicker films with larger and rougher crystal sizes with deeper grain boundaries, as shown in Fig. 1e–h and S5, S6† and we know that its surface is not the ideal location for OA anchoring. In fact, humidity can seep into the deeper boundaries, creating hydrated intermediates with the deeper MAI sites of grain boundaries of the films despite being surface terminated by PbI$_2$. Hence, as detailed in the Experimental section, we experimented with a more extensive and prolonged treatment by dipping the BC-1 films in the oleic acid solution instead of spin coating. The stability of the films was significantly enhanced, as shown in Fig. 8. As oleic acid molecules bind to Pb^{2+} or MAI$^+$ sites, the formation of hydrated

intermediates and the deprotonation of MA are hindered, causing these degradation processes to slow down dramatically.

In summary, using oleic acid for surface treatment is a cost-effective and efficient method to improve the stability of perovskite films and enhance their charge transport properties by passivating surface defects. However, this treatment must be customized to account for the specific film-forming properties of various deposition techniques. Our research showed that applying oleic acid through spin coating yields superior results on smoother perovskite films with finer grain boundaries, in contrast to textured films with larger crystals and deeper grain boundaries. Furthermore, surface termination significantly influences treatment effectiveness; while extensive research has focused on enhancing the stability and efficiency of spin-coated films, there has been limited exploration into films produced with large-scale manufacturing-compatible techniques. Given the challenges of scaling up high-efficiency devices from small to large formats, it is essential to re-evaluate strategies to facilitate a smoother transition to commercial production.

Data availability

All data relevant to the manuscript submitted is included in the main text and ESI† documents. If there is any more data needed, we will be happy to make it readily available.

Conflicts of interest

There are no conflicts to declare.

Acknowledgements

References

1 Y. Chen, Z. Yue, S.-W. Tsang and Y. Cheng, *Nano Energy*, 2025, **137**, 110782.

2 Best Research-Cell Efficiency Chart | Photovoltaic Research | NREL, https://www.nrel.gov/pv/cell-efficiency.html, (accessed March 9, 2025).

3 Y. Cheng and L. Ding, *Energy Environ. Sci.*, 2021, **14**, 3233–3255.

4 N. Li, X. Niu, Q. Chen and H. Zhou, *Chem. Soc. Rev.*, 2020, **49**, 8235–8286.

5 L. Duan, D. Walter, N. Chang, J. Bullock, D. Kang, S. P. Phang, K. Weber, T. White, D. Macdonald, K. Catchpole and H. Shen, *Nat. Rev. Mater.*, 2023, **8**, 261–281.

6 P. Zhu, C. Chen, J. Dai, Y. Zhang, R. Mao, S. Chen, J. Huang and J. Zhu, *Adv. Mater.*, 2024, **36**, 2307357.

7 E. H. Balaguera and J. Bisquert, *Small*, 2025, **21**, 2409534.

8 S. J. Kim, I. H. Im, J. H. Baek, S. Choi, S. H. Park, D. E. Lee, J. Y. Kim, S. Y. Kim, N.-G. Park, D. Lee, J. J. Yang and H. W. Jang, *Nat. Nanotechnol.*, 2025, **20**, 83–92.

9 J. Chen, X. Wang, T. Wang, J. Li, H. Y. Chia, H. Liang, S. Xi, S. Liu, X. Guo, R. Guo, Z. Jia, X. Yin, Q. Zhou, Y. Wang, Z. Shi, H. Zhou, D. Lai, M. Zhang, Z. Xing, W. R. Leow, W. Yan and Y. Hou, *Nat. Energy*, 2025, **10**, 181–190.

10 M. H. Miah, M. B. Rahman, M. Nur-E-Alam, M. A. Islam, M. Shahinuzzaman, M. R. Rahman, M. H. Ullah and M. U. Khandaker, *RSC Adv.*, 2025, **15**, 628–654.

11 D. B. Khadka, M. Yanagida and Y. Shirai, *Sol. Energy Mater. Sol. Cells*, 2025, **281**, 113319.

12 J. Yang, B. D. Siempelkamp, D. Liu and T. L. Kelly, *ACS Nano*, 2015, **9**, 1955–1963.

13 A. M. A. Leguy, Y. Hu, M. Campoy-Quiles, M. I. Alonso, O. J. Weber, P. Azarhoosh, M. van Schilfgaarde, M. T. Weller, T. Bein, J. Nelson, P. Docampo and P. R. F. Barnes, *Chem. Mater.*, 2015, **27**, 3397–3407.

14 Z. Song, A. Abate, S. C. Watthage, G. K. Liyanage, A. B. Phillips, U. Steiner, M. Graetzel and M. J. Heben, *Adv. Energy Mater.*, 2016, **6**, 1600846.

15 S. Cheng and H. Zhong, *J. Phys. Chem. Lett.*, 2022, **13**, 2281–2290.

16 H. Baishya, R. D. Adhikari, M. J. Patel, D. Yadav, T. Sarmah, M. Alam, M. Kalita and P. K. Iyer, *J. Energy Chem.*, 2024, **94**, 217–253.

17 Z. Song, N. Shrestha, S. C. Watthage, G. K. Liyanage, Z. S. Almutawah, R. H. Ahangharnejhad, A. B. Phillips, R. J. Ellingson and M. J. Heben, *J. Phys. Chem. Lett.*, 2018, **9**, 6312–6320.

18 Y. Gao, D. Lin, P. Liu, T. Shi and W. Xie, *Mater. Chem. Front.*, 2024, **8**, 785–799.

19 Y. Lu, Z. Si, H. Liu, Y. Ge, J. Hu, Z. Zhang, X. Mu, K. Selvakumar and M. Sui, *Chem. – Eur. J.*, 2021, **27**, 3729–3736.

20 B. Chen, S. Wang, Y. Song, C. Li and F. Hao, *Chem. Eng. J.*, 2022, **430**, 132701.

21 D. Zhang, D. Li, Y. Hu, A. Mei and H. Han, *Commun. Mater.*, 2022, **3**, 1–14.

22 A. Mahapatra, D. Prochowicz, M. M. Tavakoli, S. Trivedi, P. Kumar and P. Yadav, *J. Mater. Chem. A*, 2019, **8**, 27–54.

23 S. Abicho, B. Hailegnaw, G. A. Workneh and T. Yohannes, *Mater. Renew. Sustain. Energy*, 2022, **11**, 47–70.

24 S. Liu, Y. Guan, Y. Sheng, Y. Hu, Y. Rong, A. Mei and H. Han, *Adv. Energy Mater.*, 2020, **10**, 1902492.

25 G. Abdelmageed, H. R. Sully, S. B. Naghadeh, A. E. Ali, S. A. Carter and J. Z. Zhang, *ACS Appl. Energy Mater.*, 2018, **1**, 387–392.

26 M. Roy, M. Sykora and M. Aslam, *Top. Curr. Chem.*, 2024, **382**, 9.

27 J. Zhang, R. W. Crisp, J. Gao, D. M. Kroupa, M. C. Beard and J. M. Luther, *J. Phys. Chem. Lett.*, 2015, **6**, 1830–1833.

28 A. Maxwell, H. Chen, L. Grater, C. Li, S. Teale, J. Wang, L. Zeng, Z. Wang, S. M. Park, M. Vafaie, S. Sidhik, I. W. Metcalf, Y. Liu, A. D. Mohite, B. Chen and E. H. Sargent, *ACS Energy Lett.*, 2024, **9**, 520–527.

29 M. M. Hasan, C. Clegg, M. Manning, A. El Ghanam, C. Su, M. D. Harding, C. Bennett, I. G. Hill and G. I. Koleilat, *ACS Photonics*, 2020, **7**, 57–67.

30 B. T. Smith, S. T. Thornton, G. Abdelmageed, R. F. Kahwagi, R. Elsebai, V. Chiriac, C.-Y. Kim, S. Hinds and G. I. Koleilat, *Adv. Photonics Res.*, 2023, **4**, 2200088.

31 M. Wang, Y. Feng, J. Bian, H. Liu and Y. Shi, *Chem. Phys. Lett.*, 2018, **692**, 44–49.

32 T.-S. Su, T.-E. Fan, H.-K. Si, D.-A. Le, N. Perumbalathodi and T.-C. Wei, *Sol. RRL*, 2021, **5**, 2100109.

33 L. Greenspan, *J. Res. Natl. Bur. Stand., Sect. A*, 1977, **81**, 89–96.

34 A. Wexler and S. Hasegawa, *J. Res. Natl. Bur. Stand.*, 1954, **53**, 19.

35 Y. Shao, Z. Xiao, C. Bi, Y. Yuan and J. Huang, *Nat. Commun.*, 2014, **5**, 5784.

36 A. F. G. Leontowich, A. Gomez, B. D. Moreno, D. Muir, D. Spasyuk, G. King, J. W. Reid, C.-Y. Kim and S. Kycia, *J. Synchrotron Radiat.*, 2021, **28**, 961–969.

37 N. Fairley, V. Fernandez, M. Richard-Plouet, C. Guillot-Deudon, J. Walton, E. Smith, D. Flahaut, M. Greiner, M. Biesinger, S. Tougaard, D. Morgan and J. Baltrusaitis, *Appl. Surf. Sci. Adv.*, 2021, **5**, 100112.

38 H. Xie, X. Liu, L. Lyu, D. Niu, Q. Wang, J. Huang and Y. Gao, *J. Phys. Chem. C*, 2016, **120**, 215–220.

39 G. Greczynski and L. Hultman, *J. Appl. Phys.*, 2022, **132**, 011101.

40 M. He, B. Li, X. Cui, B. Jiang, Y. He, Y. Chen, D. O'Neil, P. Szymanski, M. A. Ei-Sayed, J. Huang and Z. Lin, *Nat. Commun.*, 2017, **8**, 16045.

41 J. Xia, C. Liang, S. Mei, H. Gu, B. He, Z. Zhang, T. Liu, K. Wang, S. Wang, S. Chen, Y. Cai and G. Xing, *J. Mater. Chem. A*, 2021, **9**, 2919–2927.

42 H. Kim, J. Lee, B. Kim, H. R. Byun, S. H. Kim, H. M. Oh, S. Baik and M. S. Jeong, *Sci. Rep.*, 2019, **9**, 15461.

43 J. A. Christians, P. A. M. Herrera and P. V. Kamat, *J. Am. Chem. Soc.*, 2015, **137**, 1530–1538.

44 K. Yao, X. Wang, F. Li and L. Zhou, *Chem. Commun.*, 2015, **51**, 15430–15433.

45 A. Z. Chen, B. J. Foley, J. H. Ma, M. R. Alpert, J. S. Niezgoda and J. J. Choi, *J. Mater. Chem. A*, 2017, **5**, 7796–7800.

46 N.-K. Kim, Y. H. Min, S. Noh, E. Cho, G. Jeong, M. Joo, S.-W. Ahn, J. S. Lee, S. Kim, K. Ihm, H. Ahn, Y. Kang, H.-S. Lee and D. Kim, *Sci. Rep.*, 2017, **7**, 4645.

47 H.-H. Huang, Z. Ma, J. Strzalka, Y. Ren, K.-F. Lin, L. Wang, H. Zhou, Z. Jiang and W. Chen, *Cell Rep. Phys. Sci.*, 2021, **2**, 100395.

48 M. Qin, H. Xue, H. Zhang, H. Hu, K. Liu, Y. Li, Z. Qin, J. Ma, H. Zhu, K. Yan, G. Fang, G. Li, U.-S. Jeng, G. Brocks, S. Tao and X. Lu, *Adv. Mater.*, 2020, **32**, 2004630.

49 G. Abdelmageed, L. Jewell, K. Hellier, L. Seymour, B. Luo, F. Bridges, J. Z. Zhang and S. Carter, *Appl. Phys. Lett.*, 2016, **109**, 233905.

50 Y. Zheng, Y. Cui and W. Wang, *Minerals*, 2018, **8**, 341.

51 J. Yang, Q. Hong, Z. Yuan, R. Xu, X. Guo, S. Xiong, X. Liu, S. Braun, Y. Li, J. Tang, C. Duan, M. Fahlman and Q. Bao, *Adv. Opt. Mater.*, 2018, **6**, 1800262.

52 T. Glaser, C. Müller, M. Sendner, C. Krekeler, O. E. Semonin, T. D. Hull, O. Yaffe, J. S. Owen, W. Kowalsky, A. Pucci and R. Lovrinčić, *J. Phys. Chem. Lett.*, 2015, **6**, 2913–2918.

53 G. Abdelmageed, C. Mackeen, K. Hellier, L. Jewell, L. Seymour, M. Tingwald, F. Bridges, J. Z. Zhang and S. Carter, *Sol. Energy Mater. Sol. Cells*, 2018, **174**, 566–571.

54 T. Vincent, C. Vincent, Y. Barré, Y. Guari, G. L. Saout and E. Guibal, *J. Mater. Chem. A*, 2014, **2**, 10007–10021.

55 W. A. P. J. Premaratne, W. M. G. I. Priyadarshana, S. H. P. Gunawardena and A. A. P. D. Alwis, *J. Sci. Univ. Kelaniya*, 2014, **8**, 33–48.

56 D. Yerezhep, Z. Omarova, A. Aldiyarov, A. Shinbayeva and N. Tokmoldin, *Molecules*, 2023, **28**, 1288.

57 Z. Gan, Z. Yu, M. Meng, W. Xia and X. Zhang, *APL Mater.*, 2019, **7**, 031107.

58 J. Ibarra, J. Melendres, M. Almada, M. G. Burboa, P. Taboada, J. Juárez and M. A. Valdez, *Mater. Res. Express*, 2015, **2**, 095010.

59 M. Z. Hossain, A. K. Jhawar, M. B. I. Chowdhury, W. Z. Xu, W. Wu, D. V. Hiscott and P. A. Charpentier, *Energy Fuels*, 2017, **31**, 4013–4023.

60 J. J. Nájera and A. B. Horn, *Phys. Chem. Chem. Phys.*, 2009, **11**, 483–494.

61 H. Chen, X. Ding, P. Xu, T. Hayat, A. Alsaedi, J. Yao, Y. Ding and S. Dai, *ACS Appl. Mater. Interfaces*, 2018, **10**, 1781–1791.

62 A. D. Sheikh, A. P. Patil, S. S. Mali, C. K. Hong and P. S. Patil, *J. Mater. Sci.*, 2019, **54**, 10825–10835.

63 C. Rocks, V. Svrcek, P. Maguire and D. Mariotti, *J. Mater. Chem. C*, 2017, **5**, 902–916.

64 Z. Ahmad, M. A. Najeeb, R. A. Shakoor, A. Alashraf, S. A. Al-Muhtaseb, A. Soliman and M. K. Nazeeruddin, *Sci. Rep.*, 2017, **7**, 15406.